Accurate H_2 Sorption Modeling in *rht*-MOF NOTT-112 Using Explicit Polarization

Douglas Franz,[†] Katherine A. Forrest,[†] Tony Pham,[*,†] and Brian Space[*,†]
[†]*Department of Chemistry, University of South Florida,*
4202 East Fowler Avenue, CHE205, Tampa, FL 33620-5250, United States
[*]brian.b.space@gmail.com; tpham4@mail.usf.edu

Grand Canonical Monte Carlo

Simulations of hydrogen sorption in NOTT-112 were performed using grand canonical Monte Carlo (GCMC) on a single unit cell of the MOF (47.005 × 47.005 × 47.005 Å, containing 2,784 atoms). This method constrains the chemical potential (μ), volume (V), and temperature (T) of the MOF–sorbate system to be constant while allowing other thermodynamic quantities to fluctuate.[1] The simulation involves randomly inserting, deleting, translating, or rotating a sorbate molecule with acceptance or rejection based on a random number generator scaled by the energetic favorability of the move. An infinitely extended crystal environment was approximated by periodic boundary conditions with a spherical cut-off corresponding to half the shortest unit cell dimension length (23.5025 Å). All MOF atoms were constrained to be rigid for the simulations. In GCMC, the average particle number was calculated by the following expression:[2,3]

$$\langle N \rangle = \frac{1}{\Xi} \sum_{N=0}^{\infty} e^{\beta \mu N} \left\{ \prod_{i=1}^{3N} \int_{-\infty}^{\infty} dx_i \right\} N e^{-\beta U(x_1, \ldots x_{3N})} \tag{1}$$

where Ξ is the grand canonical partition function, β is the quantity $1/kT$ (k is the Boltzmann constant), and U is the total potential energy. The chemical potential for hydrogen was determined using the BACK equation of state.[4] The total potential energy of the MOF–sorbate system was calculated by summing the repulsion/dispersion energy, the electrostatic energy, and the many-body polarization energy. Once $\langle N \rangle$ was calculated, it was converted to a value that can be compared with experiment, which is weight percent (wt %) in this case, defined as: [(Mass of H_2)/(Mass of MOF + Mass of H_2)] × 100%.

For the simulations of hydrogen sorption at the temperatures considered in this work, quantum mechanical dispersion effects were included semiclassically through the fourth order Feynman-Hibbs correction according to the following equation:[5]

$$U_{FH} = U + \frac{\beta \hbar^2}{24\mu} \left(U'' + \frac{2}{r} U' \right) + \frac{\beta^2 \hbar^4}{1152 \mu^2} \left(\frac{15}{r^3} U' + \frac{4}{r} U''' + U'''' \right) \tag{2}$$

where $\hbar$ is the reduced Planck's constant and the primes indicate differentiation with respect to pair separation r.

The isosteric heat of adsorption (Q_{st}) values were calculated based on the fluctuations in the particle number and the total potential energy in the system through the following expression:[6]

$$Q_{st} = -\frac{\langle NU \rangle - \langle N \rangle \langle U \rangle}{\langle N^2 \rangle - \langle N \rangle^2} + kT \tag{3}$$

For all state points considered, the simulations consisted of a minimum of 2.5×10^5 Monte Carlo (MC) steps to guarantee equilibration. For the first charge parametrization, the average of ≥ 4 post-equilibration serial simulations was used for the state points. For the second charge parametrization, the final average of 6 parallel simulations accounting for $\geq 1 \times 10^5$ MC steps was used. All simulations used a correlation time of 1×10^3 MC steps in order to produce uncorrelated equilibrium configurations. The choice of an average of post-equilibrated serial state points or parallel post-equilibrated state points had trivial differences in the final value (e.g., < 0.01 wt % for uptake isotherms). All simulations were performed using the Massively Parallel Monte Carlo (MPMC) code,[7] which is currently available for download on GitHub.

Many-Body Polarization

An overview of the Thole-Applequist type polarization model[8–10] used in this work is given here. The induced dipole, μ, at site i can be calculated using the following equation:

$$\vec{\mu}_i = \alpha_i^\circ \left(\vec{E}_i^{stat} - \sum_{j \neq i}^{N} \mathbf{T}_{ij} \vec{\mu}_j \right) \tag{4}$$

where α_i° represents the atomic point polarizability, $\vec{E}_i^{stat}$ is the static electric field felt at site i due to the presence of the MOF atoms and the sorbate molecules, $\vec{\mu}_j$ represents the induced dipole at site j, and $\mathbf{T}_{ij}^{\alpha\beta}$ is the dipole field tensor which is defined from first-principles as the following:[8]

$$\mathbf{T}_{ij}^{\alpha\beta} = \nabla^\alpha \nabla^\beta \frac{1}{r_{ij}} \tag{5}$$

$$= \frac{\delta^{\alpha\beta}}{r_{ij}^3} - \frac{3x^\alpha x^\beta}{r_{ij}^5} \tag{6}$$

where r_{ij} is the distance between sites i and j. Equation 4 is a self-consistent field equation with respect to the dipoles and thus, the quantity $\vec{\mu}_i$ must be solved for using iterative methods for large systems. The iterative method employed herein was the Gauss–Seidel relaxation technique.[11] This method consists of updating the current dipole vector set for the kth iteration step as the new dipole vectors become available *via* the following:[12]

$$\vec{\mu}_i^k = \alpha_i^\circ \left(\vec{E}_i^{stat} - \sum_{j \neq i} \hat{T}_{ij} \vec{\mu}_j^{k-1+\zeta} \right) \tag{7}$$

$$\zeta = \begin{cases} 0, & \text{if } i < j \\ 1, & \text{if } i > j \end{cases} \tag{8}$$

In this equation, $\hat{T}_{ij}$ is the modified dipole field tensor that accounts for short range divergences in the polarization model, defined as:[12–14]

$$\hat{T}_{ij}^{\alpha\beta} = \frac{\delta_{\alpha\beta}}{r_{ij}^3} \left[1 - \left(\frac{\lambda^2 r_{ij}^2}{2} + \lambda r_{ij} + 1 \right) e^{-\lambda r_{ij}} \right] - \frac{3x^\alpha x^\beta}{r_{ij}^5} \left[1 - \left(\frac{\lambda^3 r_{ij}^3}{6} + \frac{\lambda^2 r_{ij}^2}{2} + \lambda r_{ij} + 1 \right) e^{-\lambda r_{ij}} \right] \tag{9}$$

where λ is a parameter damping the dipole interactions near the regions of discontinuity. A value of 2.1304 was used for λ in this work, which is consistent with the work performed by B. Thole.[9] The many-body polarization energy for the MOF–H_2 system was calculated by the following based on the work of Palmo and Krimm:[15]

$$U_{pol}^k = -\frac{1}{2} \sum_i \vec{\mu}_i^k \cdot \vec{E}_i^{stat} - \frac{1}{2} \sum_i \vec{\mu}_i^k \cdot \vec{E}_i^{k+1} \tag{10}$$

Thus, the polarization energy was determined from the kth iteration dipoles and the $(k+1)^{th}$ induced field. In the case of simulations of H_2 sorption in NOTT-112 with the BSSP model, k was equal to 4.

Simulated Annealing

Simulated annealing calculations within the canonical ensemble (NVT) were performed on the MOF–H_2 system at various starting temperatures (20, 40, 77, and 1000 K) using the BSSP model for H_2 and D_2. For the latter, the only difference is the modified atomic mass in the model; otherwise, all parameters associated with the BSSP hydrogen model remained unchanged (Table S7)). A generalized procedure for simulated annealing is provided by Kirkpatrick *et al.*[16] In this work, the temperature was scaled by a factor of 0.99999 after every 1×10^3 Monte Carlo steps. The starting positions of the sorbate molecules were located approximately 2.5 Å from the CuC or CuL ions, with the molecule oriented perpendicularly to the Cu–Cu axis of the copper paddlewheels.

NOTT-112 Unit Cell and Components

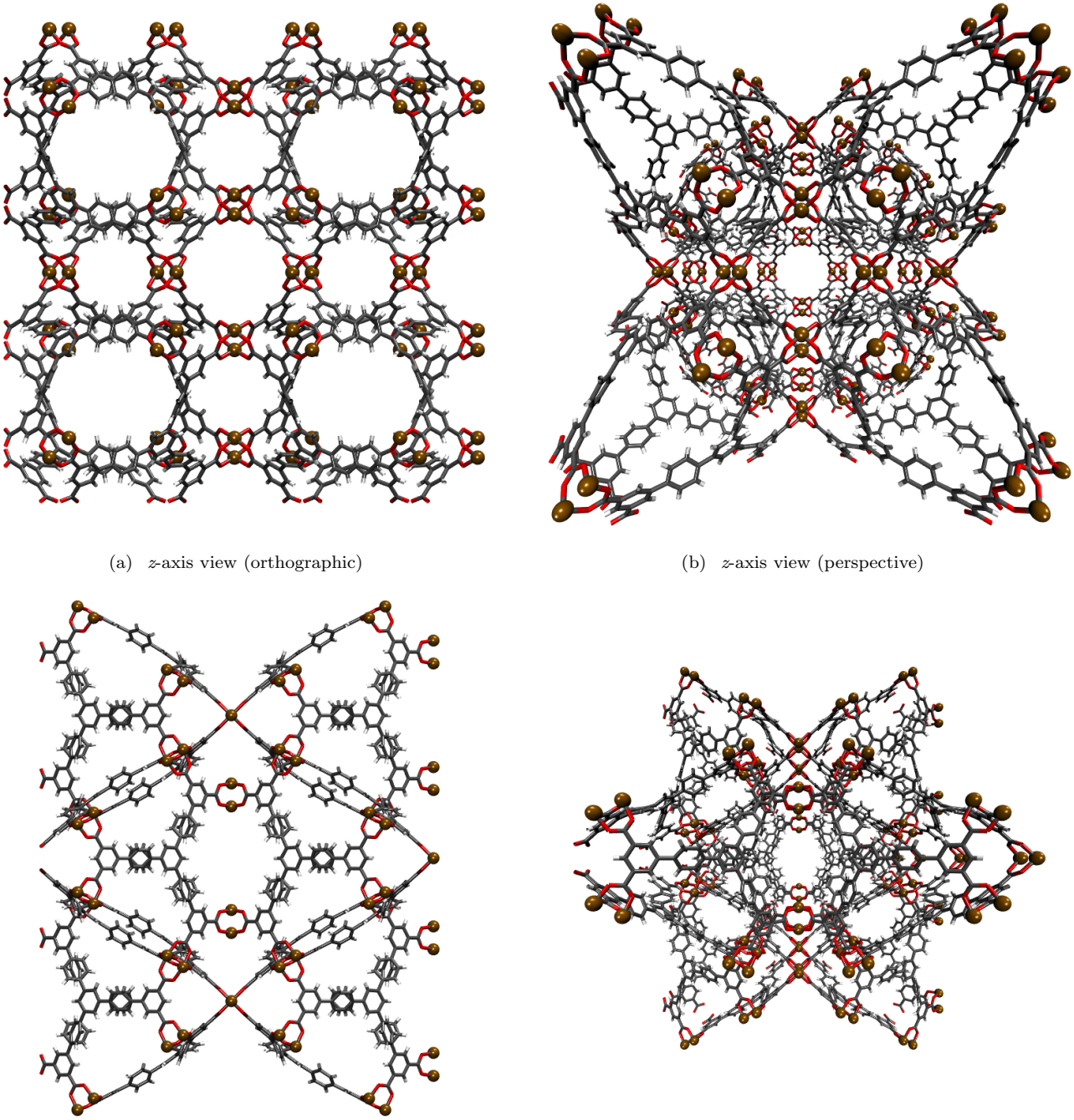

(a) z-axis view (orthographic)

(b) z-axis view (perspective)

(c) Rotation along the x-axis by 45° (orthographic)

(d) Rotation along the x-axis by 45° (perspective)

Figure S1. Molecular views of the unit cell of NOTT-112 as determined by X-ray crystallography data.[17] Atom Colors: Cu = brown; O = red; C = grey; H = white.

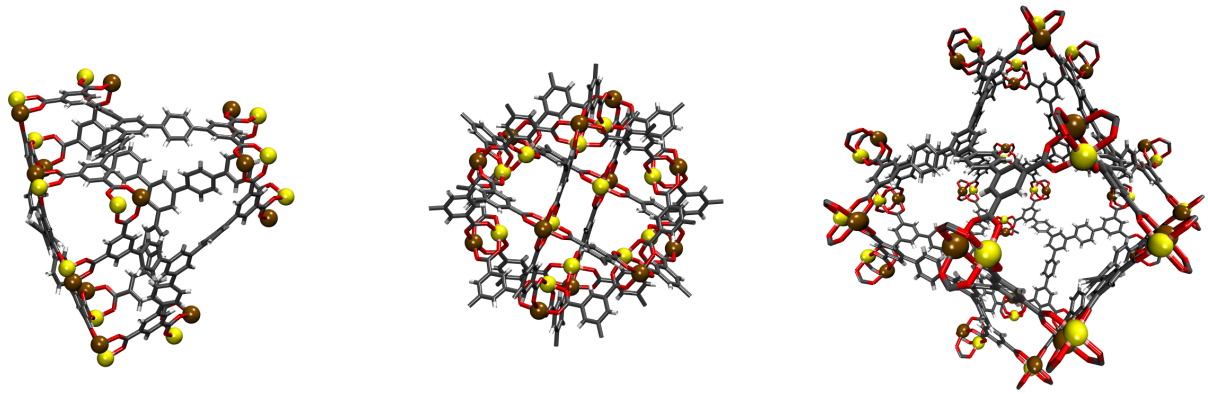

(a) Truncated Tetrahedron (T–T_d) (b) Cuboctahedron (cub–O_h) (c) Truncated Octahedron (T–O_h)

Figure S2. The three unique cages observed in the crystal structure of NOTT-112. Note, the two chemically distinct Cu^{2+} ions are shown in different colors. Atom colors: CuC = yellow; CuL = brown; O = red; C = grey; H = white.

NOTT-112 Fragments

Figure S3. Representational gas phase fragments of NOTT-112 that were selected for charge-fitting calculations. Atom colors: Cu = brown; O = red; C = cyan; H = white.

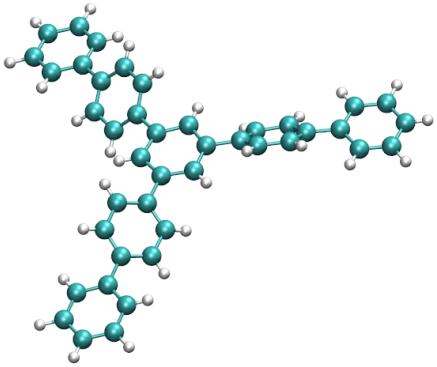

(a) Fragment 1

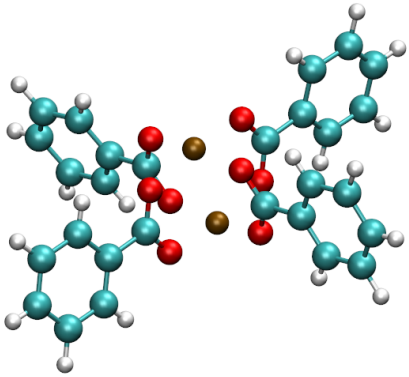

(b) Fragment 2

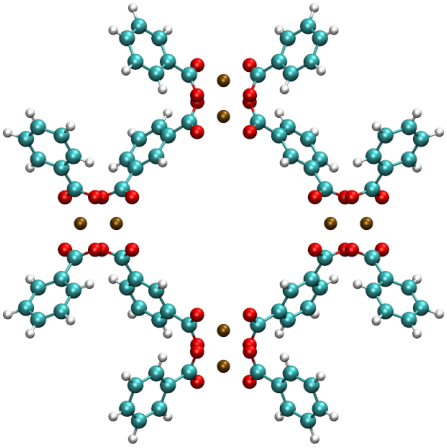

(c) Fragment 3

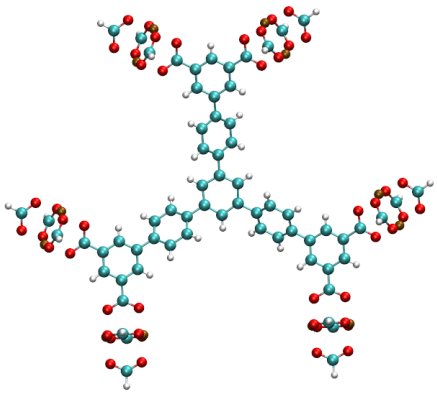

(d) Fragment 4

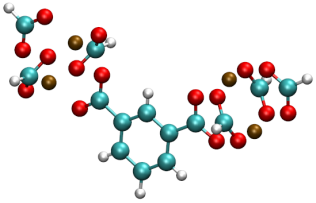

(e) Fragment 5

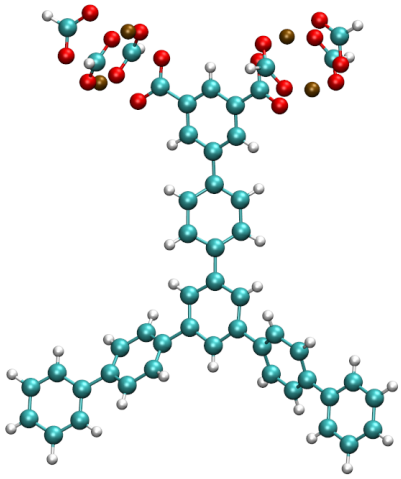

(f) Fragment 6

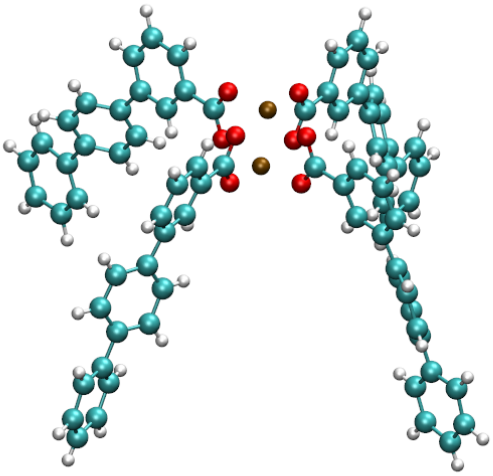

(g) Fragment 7

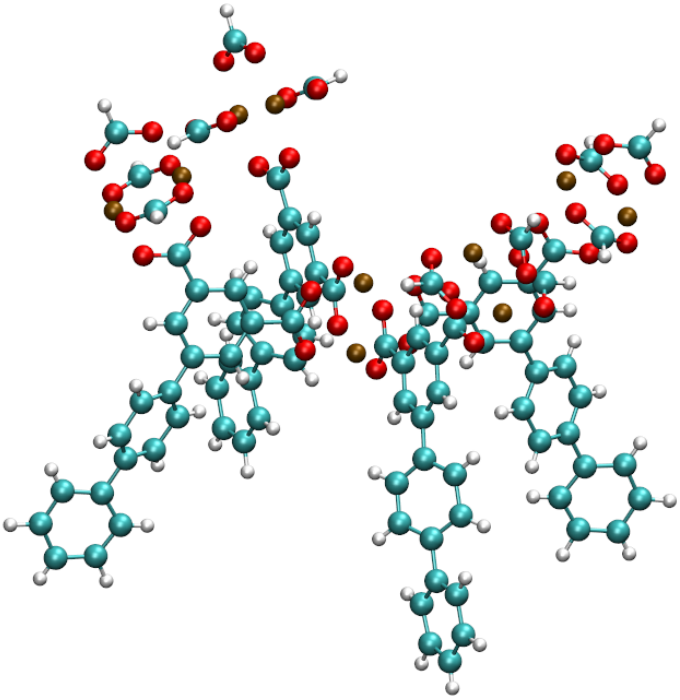

(h) Fragment 8

MOF and H_2 Simulation Parameters

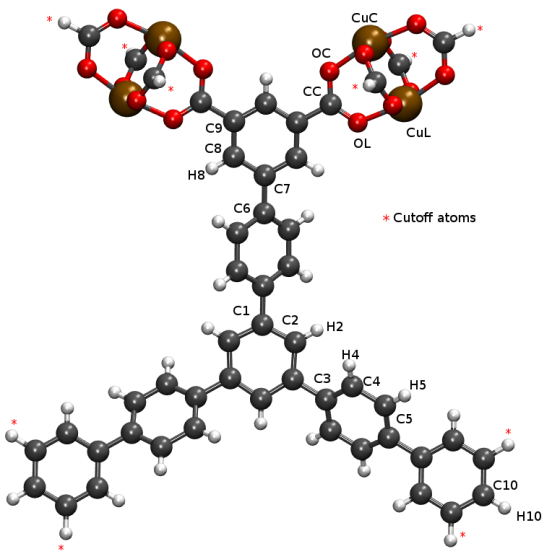

Figure S4. The numbering of the chemically distinct atoms in NOTT-112 as referred to in Tables S1, S2, S4 and S5. Fragment 6 (Figure S3(f)) is pictured here. Atom colors: Cu = brown; O = red; C = grey; H = white.

Table S1. Average calculated partial charges (in e^-) for the chemically distinct atoms in NOTT-112 for the first charge parametrization in this study, where all C, H, and O atoms were treated with the 6-31G* basis set and the Cu^{2+} ions were treated with the LANL2DZ ECP basis set. The standard deviation (S.D.) of the calculated partial charges for each chemically distinct atom from the eight fragments are also provided. Labeling of atoms correspond to Figure S4.

Atom #	Atom ID	# in unit-cell	q (e^-)	S.D.
1	CuC	48	1.34507	0.058
2	CuL	48	0.85731	0.133
3	OC	192	-0.72200	0.043
4	OL	192	-0.73515	0.047
5	CC	192	0.93237	0.055
6	C1	96	0.17032	0.007
7	C2	96	-0.37263	0.017
8	C3	96	0.07059	0.018
9	C4	192	0.17122	0.011
10	C5	192	-0.18739	0.036
11	C6	96	0.07101	0.034
12	C7	96	0.04139	0.052
13	C8	192	-0.11308	0.049
14	C9	192	-0.14962	0.014
15	C10	96	-0.10868	0.037
16	H2	96	0.21382	0.003
17	H4	192	0.13495	0.007
18	H5	192	0.14701	0.013
19	H8	192	0.17365	0.015
20	H10	96	0.19395	0.014
	Total:	2784		

Table S2. Average calculated partial charges (in e^-) for the chemically distinct atoms in NOTT-112 for the second charge parametrization in this study, where **all** atoms were treated with the 6-31G* basis set. The standard deviation (S.D.) of the calculated partial charges for each chemically distinct atom from the eight fragments are also provided. Further, the difference in charge magnitude from the first charge parametrization for all unique atoms are included. Labeling of atoms correspond to Figure S4.

Atom #	Atom ID	# in unit-cell	q (e^-)	S.D.	Diff. from param. 1
1	CuC	48	1.55821	0.045	+0.213
2	CuL	48	0.99787	0.083	+0.141
3	OC	192	-0.77791	0.023	-0.056
4	OL	192	-0.77102	0.028	-0.036
5	CC	192	0.96595	0.046	+0.034
6	C1	96	0.16290	0.016	-0.007
7	C2	96	-0.36997	0.015	+0.003
8	C3	96	0.08409	0.033	+0.014
9	C4	192	-0.17196	0.010	-0.001
10	C5	192	-0.18237	0.035	+0.005
11	C6	96	0.07351	0.035	+0.003
12	C7	96	0.06791	0.088	+0.027
13	C8	192	-0.11098	0.085	+0.002
14	C9	192	-0.19405	0.043	-0.044
15	C10	96	-0.03305	0.037	+0.076
16	H2	96	0.21462	0.002	+0.001
17	H4	192	0.13570	0.006	+0.001
18	H5	192	0.13979	0.012	-0.007
19	H8	192	0.15233	0.009	-0.021
20	H10	96	0.15099	0.014	-0.043
	Total:	2784			

Table S3. Average calculated partial charges (in e^-) for the CuC and CuL ions from quantum mechanical calculations on Fragment 3 (Figure S3(c)) using different methods (Hartree–Fock (HF) and density functional theory (DFT)) and basis sets. Here, ECP denotes that the LANL2DZ effective core potential basis set was used for the Cu^{2+} ions only, whereas the indicated basis set was used for all other atoms. The below charges are presented as the average of the four instances of CuC and CuL for the fragment. The standard deviations for the calculated partial charges were negligable.

Method and Basis Set	CuC	CuL	CuC/CuL ratio
HF 6-31G* ECP	1.2660	0.6870	1.84
HF 6-31G ECP	1.2903	0.7785	1.66
HF 6-31G	1.4067	1.2284	1.15
HF 6-31G*	1.5280	0.9120	1.68
HF STO-6G	0.4238	0.3045	1.39
HF STO-3G	0.3487	0.2303	1.51
DFT PBE0 6-31G* ECP	1.0220	0.9995	1.02
DFT PBE0 6-31G*	1.0989	1.0798	1.02
DFT PBE0 def2-SVP ECP	1.0323	1.0040	1.03
DFT PBE0 def2-SVP	1.0307	1.0062	1.02

Table S4. Comparison of partial charges (e^-) for the series of gas phase fragments of NOTT-112 as listed in Figure 3. Labeling of atoms corresponds to Figure S4. The results are presented from the **first** charge parametrization, where all C, H, and O atoms were treated with the 6-31G* basis set and the Cu^{2+} ions were treated with the LANL2DZ ECP basis set.

Atom	Label	Fragment 1	Fragment 2	Fragment 3	Fragment 4	Fragment 5	Fragment 6	Fragment 7	Fragment 8
CuC	1	-	-	1.26643	1.38892	1.39915	1.36830	-	1.3026
CuL	2	-	-	0.6872	0.9756	0.9687	0.9096	-	0.7455
OC	3	-	-0.6748	-0.7071	-0.7493	-0.7520	-0.7500	-0.6393	-0.7080
OL	4	-	-0.6732	-0.6888	-0.7832	-0.7753	-0.7559	-0.6783	-0.7164
CC	5	-	-	0.90226	0.9758	0.9940	0.9620	0.8475	0.9124
C1	6	0.1695	-	-	0.1740	-	0.1608	0.1770	-
C2	7	-0.3654	-	-	-0.3853	-	-0.3509	-	-
C3	8	0.0638	-	-	0.0898	-	0.0799	0.0488	-
C4	9	-0.1727	-	-	-0.1672	-	-0.1539	-0.1811	-
C5	10	-0.1712	-	-	-0.200	-	-0.2254	-0.1421	-
C6	11	0.0654	-	-	0.0943	-	0.0986	0.0257	-
C7	12	-	-	-	-0.0166	-	0.0827	-	0.0851
C8	13	-	-	-	-0.0582	-	-0.1550	-	-0.1212
C9	14	-	-0.1320	-0.1462	-0.1695	-0.1498	-	-	-0.1398
C10	15	-	-	-0.0838	-0.0891	-0.1067	-0.1714	-	-0.0844
H2	16	0.2174	-	-	0.2121	-	0.2120	-	-
H4	17	0.1281	-	-	0.1411	-	0.1357	-	-
H5	18	0.1335	-	-	0.1491	-	0.1585	-	-
H8	19	-	-	-	0.1699	-	0.1905	0.1544	0.1799
H10	20	-	-	0.1855	0.1892	0.1951	0.2175	-	0.1825

Table S5. Comparison of partial charges (e^-) for the series of gas phase fragments of NOTT-112 as listed in Figure 3. Labeling of atoms corresponds to Figure S4. The results are presented from **second** charge parametrization, where **all** atoms were treated with the 6-31G* basis set.

Atom	Label	Fragment 1	Fragment 2	Fragment 3	Fragment 4	Fragment 5	Fragment 6	Fragment 7	Fragment 8
CuC	1	-	1.5252	1.5276	1.5946	1.6045	1.5973	1.4863	1.5720
CuL	2	-	0.9139	0.9122	1.0654	1.0657	1.0723	0.9018	1.0538
OC	3	-	-0.7710	-0.7692	-0.7901	-0.8002	-0.8047	-0.7390	-0.7657
OL	4	-	-0.7518	-0.7488	-0.7979	-0.7924	-0.8054	-0.7360	-0.7593
CC	5	-	0.9412	0.9400	1.0048	1.0063	1.0235	0.9005	0.9454
C1	6	0.1695	-	-	0.1744	-	0.1448	-	-
C2	7	-0.3654	-	-	-0.3863	-	-0.3571	-	-
C3	8	0.0638	-	-	0.0936	-	0.1269	0.0521	-
C4	9	-0.1727	-	-	-0.1704	-	-0.1594	-0.1847	-
C5	10	-0.1712	-	-	-0.1977	-	-0.2204	-0.1395	-
C6	11	0.0654	-	-	0.1000	-	0.1006	0.0280	-
C7	12	0.1736	-	-	-0.0396	-	0.0559	0.0817	
C8	13	-0.2406	-	-	-0.0069	-	-0.0902	-0.1312	-0.0856
C9	14	-	-0.1507	-0.2096	-0.2553	-0.2078	-0.2044	-0.1239	-0.2055
C10	15	-	-	-0.0099	-0.0131	-0.0298	-0.0613	-0.0772	-
H2	16	0.2174	-	-	0.2133	-	0.2131	-	-
H4	17	0.1282	-	-	0.1393	-	0.1349	0.1405	-
H5	18	0.1335	-	-	0.1454	-	0.1541	0.1262	-
H8	19	0.1471	-	-	0.1462	-	0.1629	0.1439	0.1615
H10	20	-	-	0.1518	0.1443	0.1570	0.1737	0.1340	0.1452

Table S6. Lennard-Jones 12–6 parameters (ϵ and σ) and point polarizabilities (α°) used for the MOF atoms in the simulations in this work. The Lennard-Jones parameters for all atoms were taken from the Universal Force Field (UFF).[18] The polarizabilities for the C, H, and O atoms were taken from van Duijnen *et al.*,[19] while the value for Cu^{2+} was calculated in previous work[14] and used herein.

Atom	σ (Å)	ϵ (K)	α° (Å^3)
Cu	3.114	2.516	2.1963
O	3.118	30.19	0.8520
C	3.431	52.84	1.2886
H	2.571	22.14	0.4138

Table S7. Parameters used to characterize the Buch,[20] BSS,[21] and BSSP[21] H_2 models as well as the D_2 model used in this work. The D_2 model is based on the BSSP H_2 model where the only difference is the atomic mass. The BSS, BSSP, and D_2 models have 5 sites, where the sites including an r value are duplicated in either direction linearly from the origin. H2G and D2G represent the center-of-mass site, H2E and D2E represent the atomic locations, and H2N and D2N represent phantom Lennard-Jones sites.

Model	Site Name	r (Å)	Atomic Mass (amu)	ϵ (K)	σ (Å)	q (e^-)	α° (Å^3)
Buch	H2G	0.000	2.016	34.20000	2.96000	0.00000	0.00000
BSS	H2G	0.000	0.000	8.85160	3.22930	-0.74640	0.00000
	H2E	0.371	1.008	0.00000	0.00000	0.37320	0.00000
	H2N	0.329	0.000	4.06590	2.34060	0.00000	0.00000
BSSP	H2G	0.000	0.000	12.76532	3.15528	-0.74640	0.69380
	H2E	0.371	1.008	0.00000	0.00000	0.37320	0.00044
	H2N	0.363	0.000	2.16726	2.37031	0.00000	0.00000
D_2	D2G	0.000	0.000	12.76532	3.15528	-0.74640	0.69380
	D2E	0.371	2.014	0.00000	0.00000	0.37320	0.00044
	D2N	0.363	0.000	2.16726	2.37031	0.00000	0.00000

H_2 Sorption Results

A. First Charge Parametrization

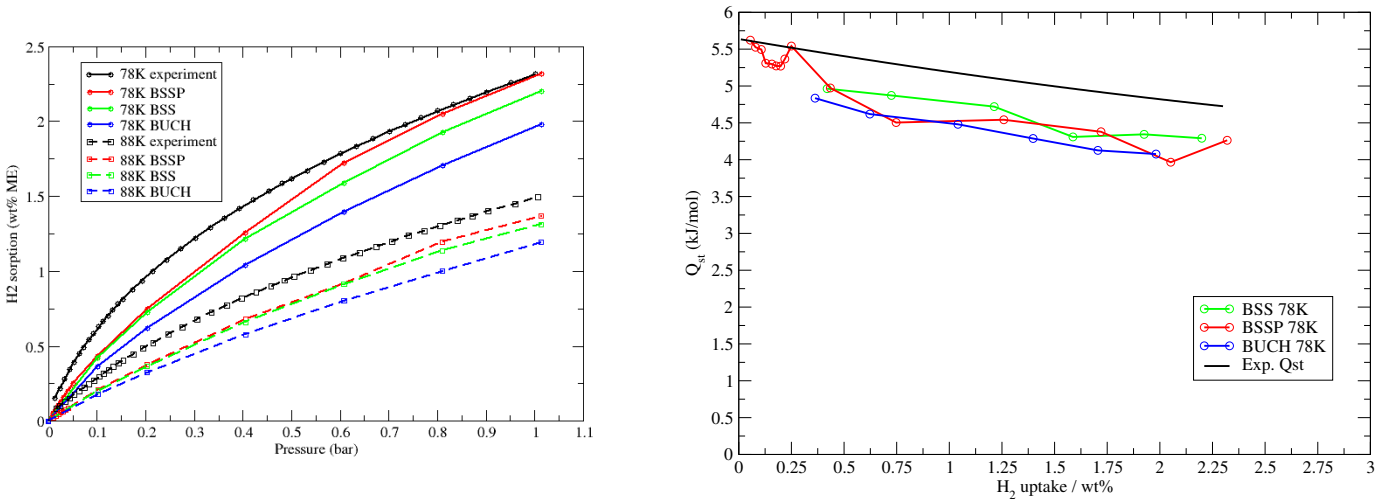

(a) (b)

Figure S5. **(a)** Low-pressure (up to ~1.0 atm) absolute H_2 sorption isotherms at 78 K (solid) and 88 K (dashed) and **(b)** isosteric heats of adsorption (Q_{st}) for H_2 in NOTT-112 for experiment (black),[17] and simulations using the BSSP (red), BSS (green), and Buch (blue) models with the **first** charge parametrization (Table S1). For the simulated isotherms, the maximum computational standard deviation of state points was about ±0.003 wt%.

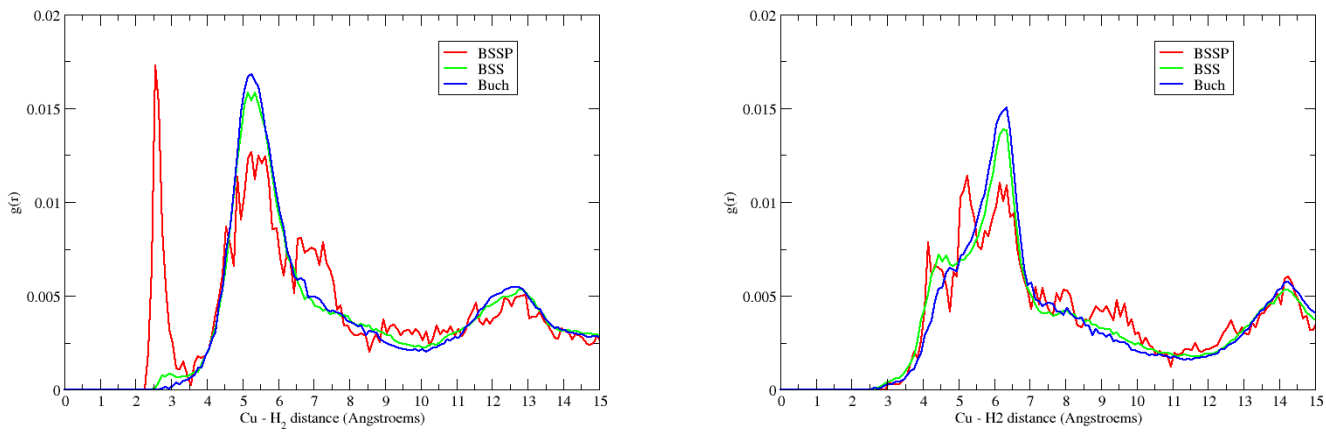

(a) (b)

Figure S6. Radial distribution function, g(r), of the center-of-mass (COM) of H_2 molecules about **(a)** the CuC ions and **(b)** the CuL ions for the BSSP (red), BSS (green), and Buch (blue) models in NOTT-112 at 78 K and 0.10 atm with the **first** charge parametrization (Table S1).

B. Second Charge Parametrization

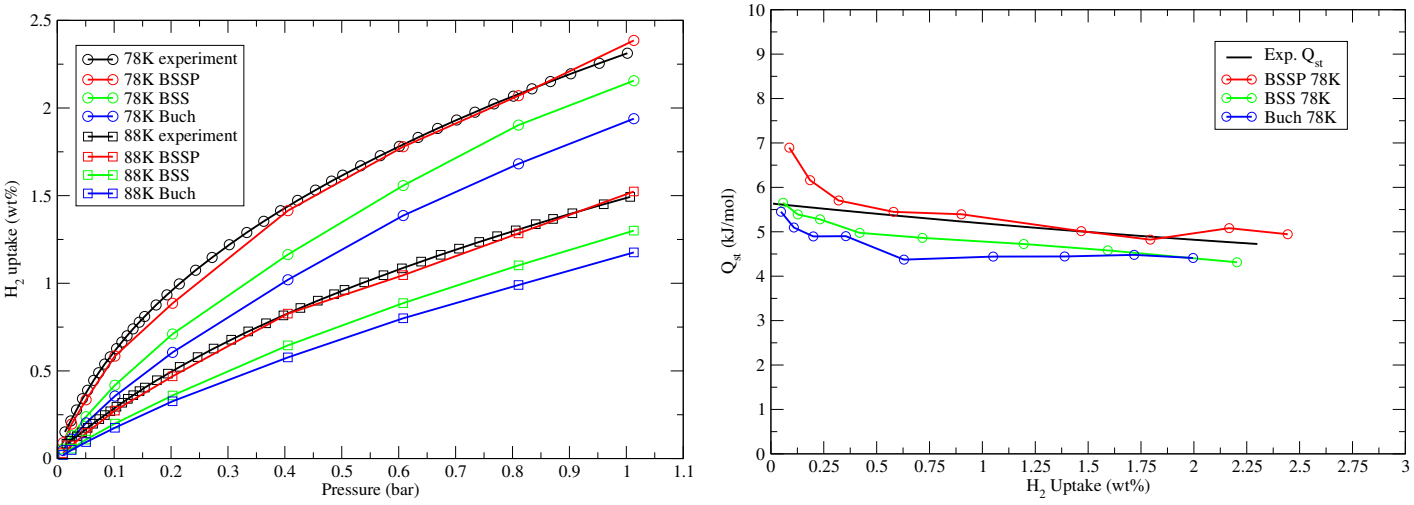

(a) (b)

Figure S7. **(a)** Low-pressure (up to ~1.0 atm) absolute H_2 sorption isotherms at 78 K (solid) and 88 K (dashed) and **(b)** isosteric heats of adsorption (Q_{st}) for H_2 in NOTT-112 for experiment (black),[17] and simulations using the BSSP (red), BSS (green), and Buch (blue) models with the **second** charge parametrization (Table S2). For the simulated isotherms, the maximum computational standard deviation of state points was about ±0.00179 wt%.

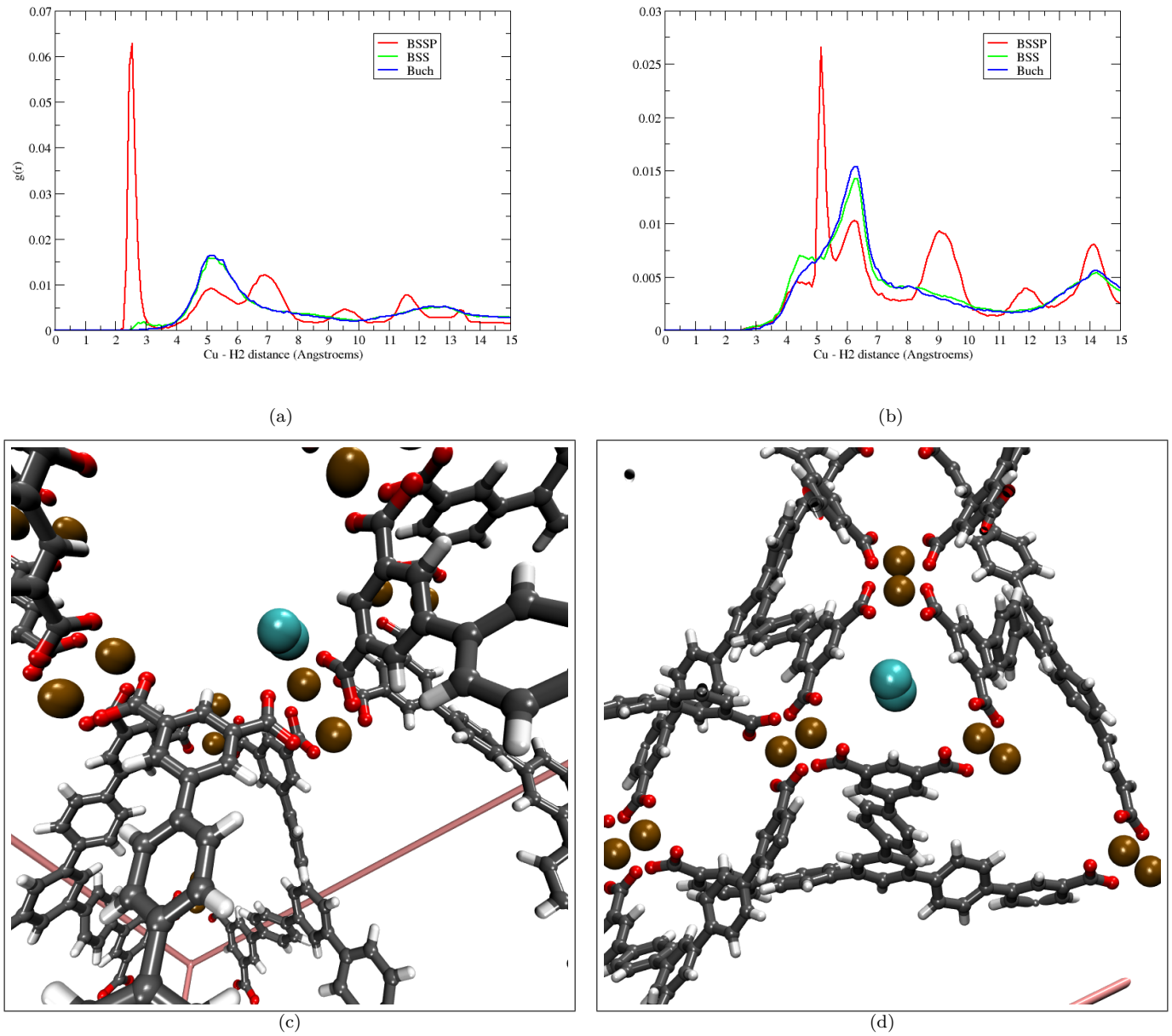

Figure S8. Radial distribution function, g(r), of the center-of-mass (COM) of H_2 molecules about **(a)** the CuC ions and **(b)** the CuL ions for the BSSP (red), BSS (green), and Buch (blue) models in NOTT-112 at 78 K and 0.10 atm with the **second** charge parametrization (Table S2). **(c)** Molecular illustration of the primary binding site about the CuC ion in NOTT-112 as captured from simulation using the BSSP model. The CuC–COM distance is ~2.5 Å. This site corresponds to the radial distribution peak with the highest intensity for the BSSP model in **(a)** and **(b)**. **(d)** Molecular illustration of the secondary binding site within the corner of the T–T_d cage in NOTT-112 as captured from simulation using all three models. The H_2 molecule is shown in cyan. MOF atom colors: Cu = brown; O = red; C = grey; H = white.

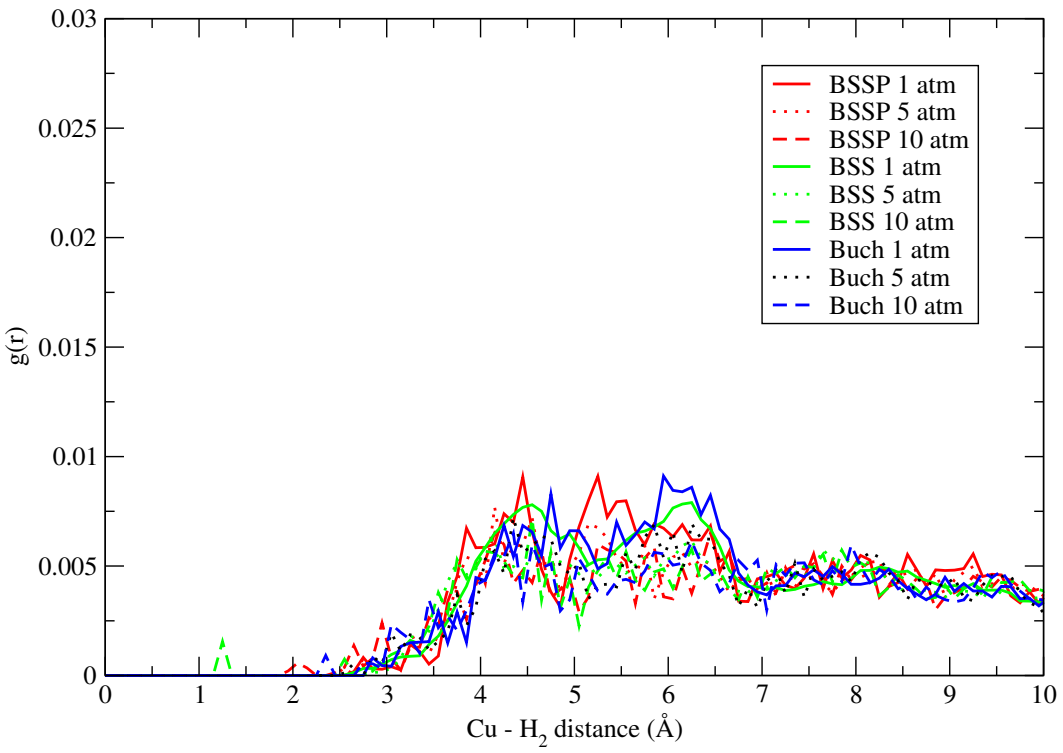

Figure S9. Radial distribution function, g(r), of the center-of-mass (COM) of H_2 molecules about **CuL** for the BSSP (red), BSS (green), and Buch (blue) models in NOTT-112 at 78 K and various pressures (1 atm = solid, 5 atm = dotted, 10 atm = dashed).

C. Induced Dipole Magnitudes and Locations

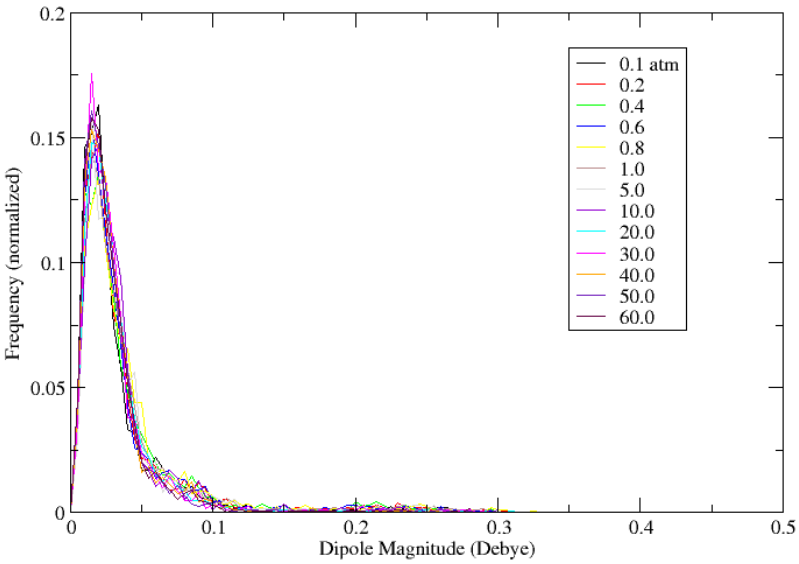

(a)

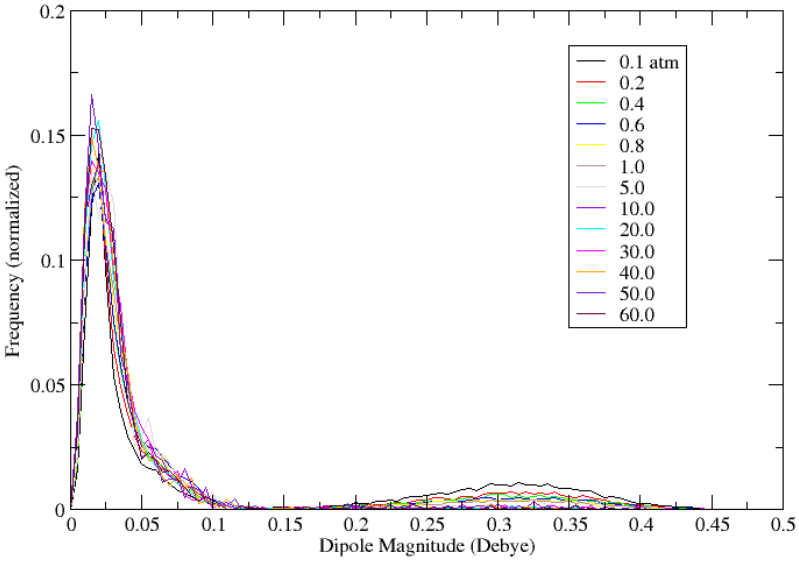

(b)

Figure S10. Normalized distribution of the induced dipole magnitudes for the BSSP model in NOTT-112 at 78 K and pressures ranging from 0.1 to 60.0 atm for the **(a) first** and **(b) second** charge parametrizations.

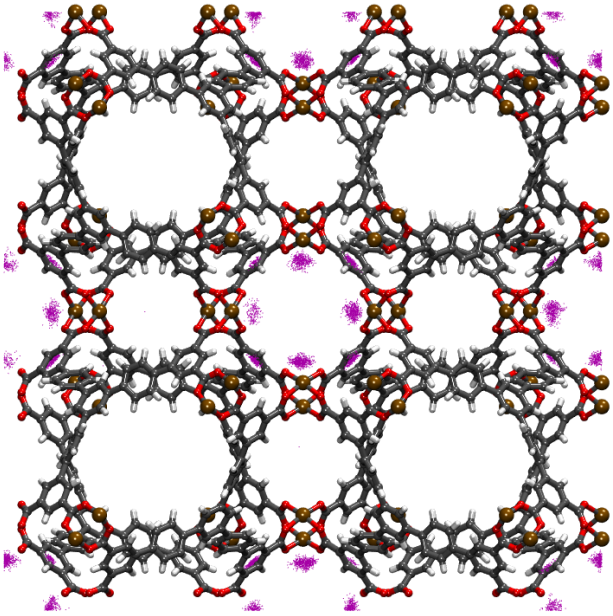

(a) z-axis view (orthographic)

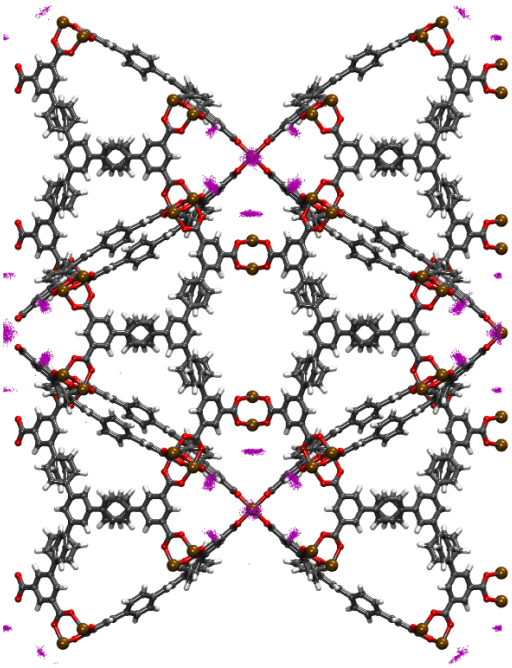

(b) Rotation along the x-axis by 45° (orthographic)

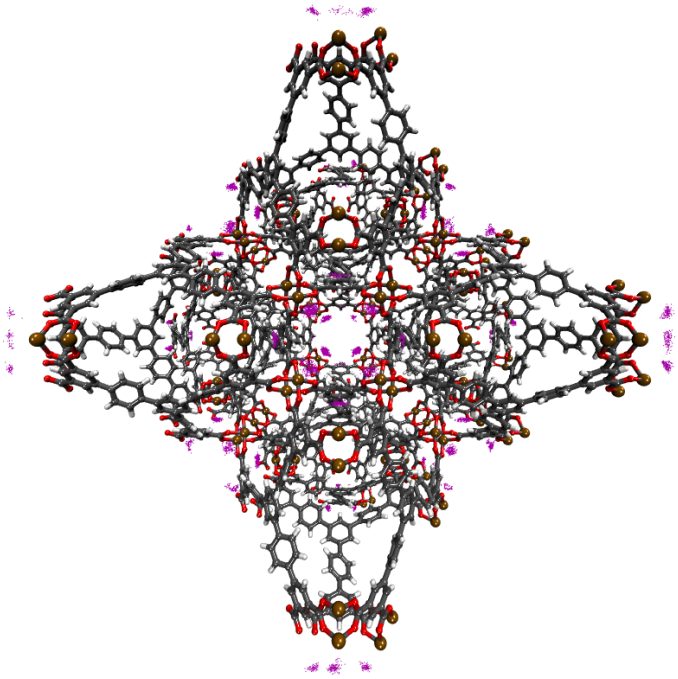

(c) z-axis view (orthographic)

Figure S11. Three views illustrating the locations of the strongest induced dipoles (0.2–0.5 Debye or 0.04–0.104 eÅ) for the BSSP H_2 molecules within NOTT-112 from the **second** charge parametrization (Figure S10(b)). Induced dipoles within this range of magnitudes are represented as purple points. The sorbate molecules with the highest induced dipoles correspond to sorption onto the CuC ions in the MOF. Atom colors: Cu = brown; O = red; C = grey; H = white.

D. H_2 Population Density Histogram

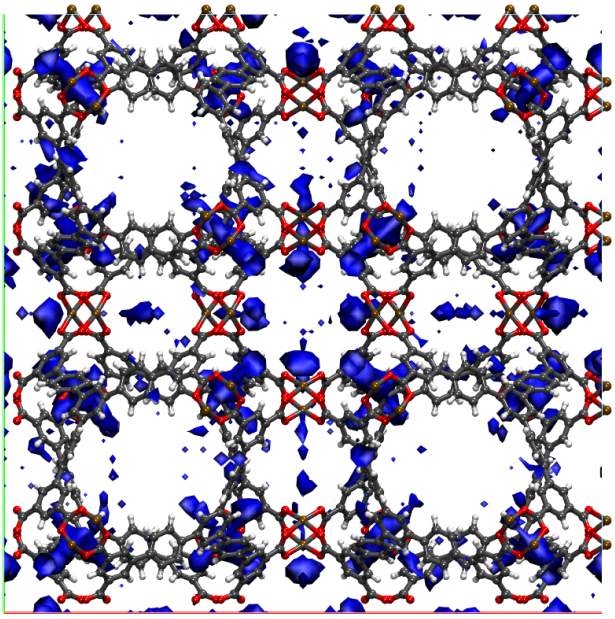

(a) z-axis view (orthographic)

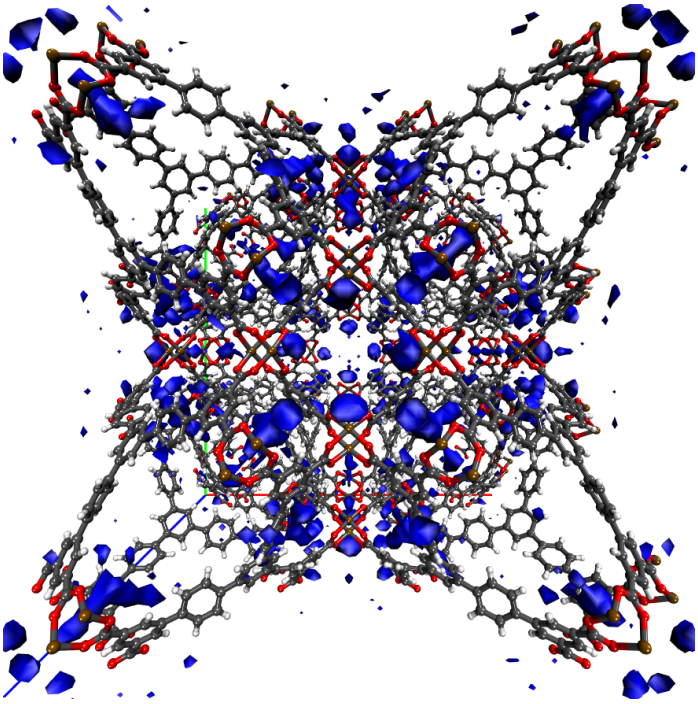

(b) z-axis view (orthographic)

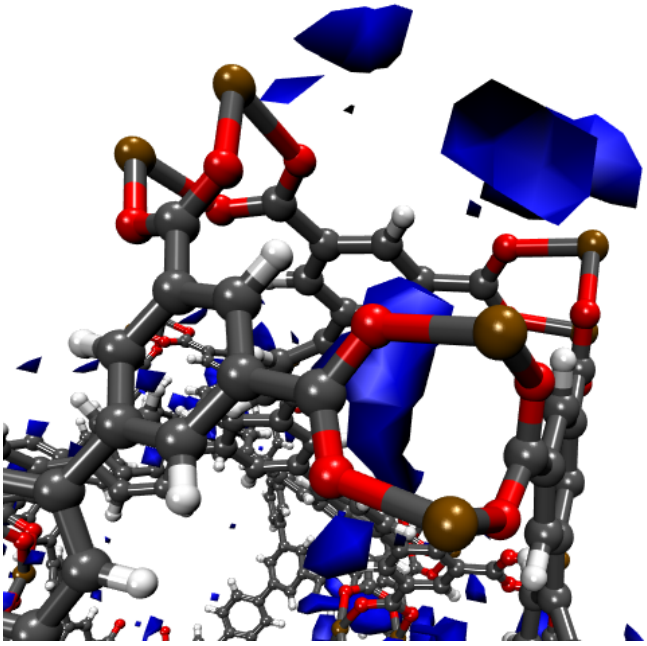

(c) Zoomed-in view of the copper paddlewheel clusters

Figure S12. Visualization of the three-dimensional H_2 molecule density histogram of the most active sorption sites (blue solids) in NOTT-112. This data was taken from simulations using the BSSP model at 78 K and 0.1 atm using the **second** charge parametrization. Atom colors: Cu = brown; O = red; C = grey; H = white.

E. Radial Distribution Function of D_2

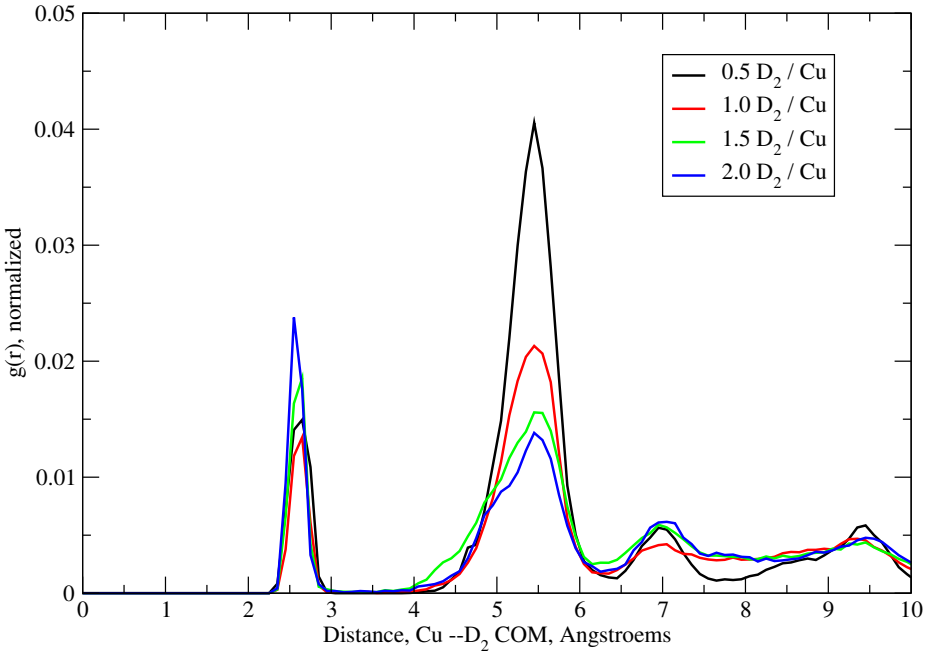

(a)

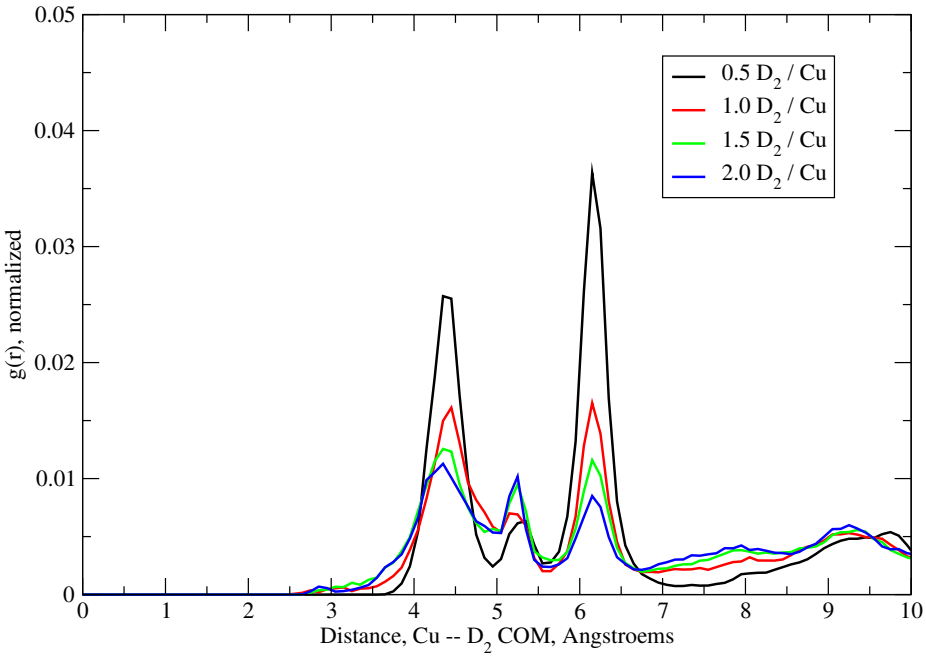

(b)

Figure S13. Radial distribution function, g(r), of the center-of-mass (COM) of D_2 molecules about **(a)** the CuC ions and **(b)** the CuL ions using the D_2 model considered in this work (Table S7) in NOTT-112 at 50 K and various loadings: 0.5 D_2/Cu (black), 1.0 D_2/Cu (red), 1.5 D_2/Cu (green), and 2.0 D_2/Cu (blue). The prominence of the first and secondary sorption sites can be observed in both **(a)** and **(b)**. The existence of a tertiary peak can be observed in **(b)** at ~5.4 Å. This peak is indicative of another experimentally determined site, nameed A4 or A5 according to reference 22.

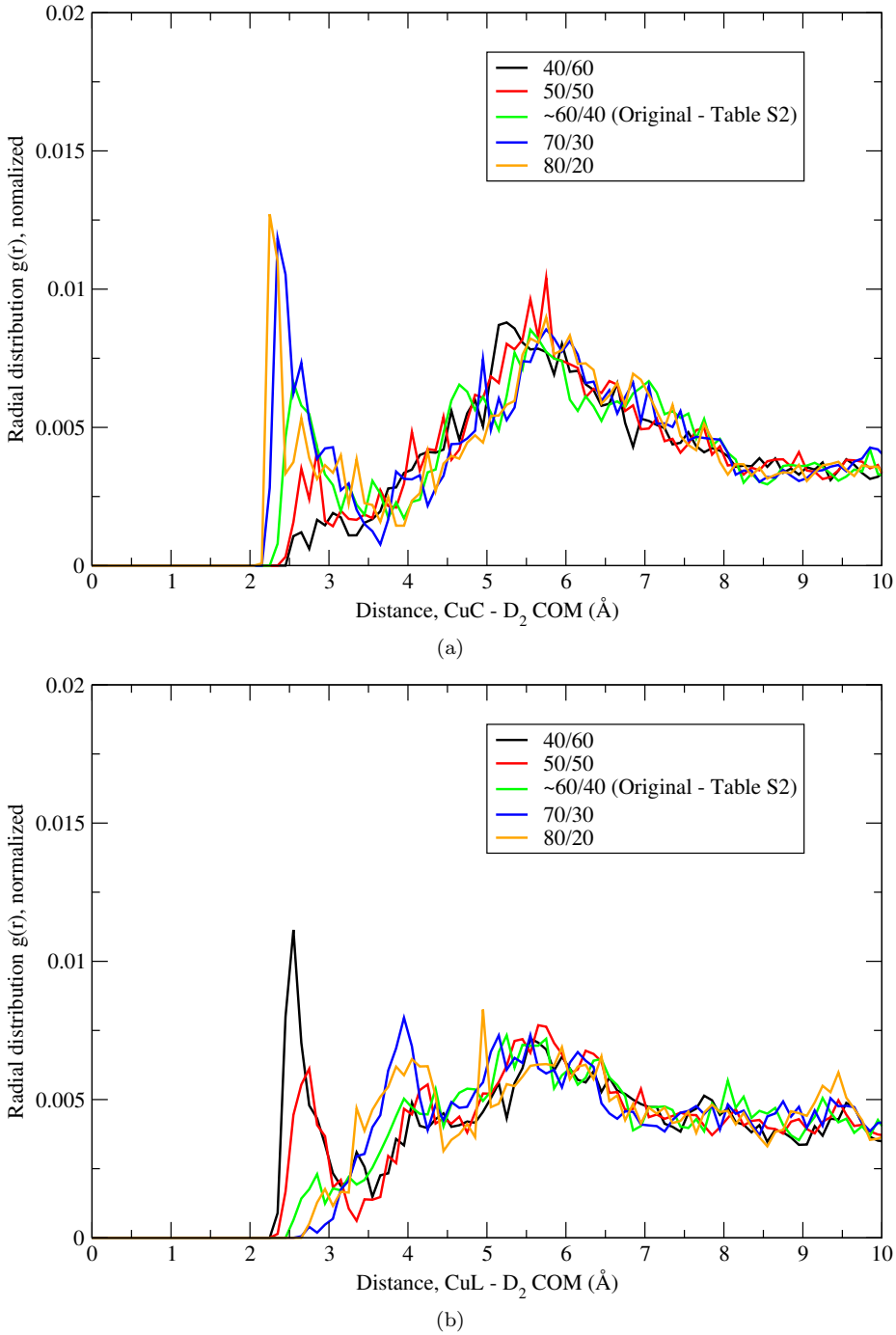

Figure S14. Radial distribution function, g(r), of the center-of-mass (COM) of D_2 molecules about **(a)** the CuC ions and **(b)** the CuL ions in simulations using the partial charges from the **second** charge parametrization (Table 2), but with manually adjusted CuC/CuL charges by fixed ratios. All simulations were performed at 50 K and 0.05 atm using the D_2 model listed in Table S7. Each g(r) is represented by a different color, where the labels indicate the relative percentages from the total that were used for CuC and CuL: 40% CuC, 60% CuL (black); 50% CuC, 50% CuL (red); ~60% CuC, ~40% CuL (green); 70% CuC, 30% CuL (blue); 80% CuC, 20% CuL (orange). Note, the ~60% CuC, ~40% CuL label epresents the original results obtained from the second charge parametrization.

Table S8. The partial charges (in e^-) that were used for the CuC and CuL ions in simulations of D_2 sorption in NOTT-112 where the charges for the respective ions were adjusted by fixed ratios. Results for the radial distribution function, g(r), from these simulations are shown in Figure 14.

CuC/CuL %	40/60	50/50	Original (~60/40)	70/30	80/20
CuC q (e^-)	1.022432	1.278040	1.558210	1.789256	2.044864
CuL q (e^-	1.533648	1.278040	0.997870	0.766824	0.511216

[1] Metropolis, N.; Rosenbluth, A. W.; Rosenbluth, M. N.; Teller, A. H.; Teller, E. *J. Chem. Phys.* **1953**, *21*, 1087–1092.
[2] McQuarrie, D. A. *Statistical Mechanics*; University Science Books: Sausalito, CA, 2000; Chapt. 3, pg. 53.
[3] Frenkel, D.; Smit, B. *Understanding Molecular Simulation: From Algorithms to Applications*; Academic Press: New York, 2002; Chapt. 5, Sect. 6.1, p.129.
[4] Boublík, T. *Fluid Phase Equil.* **2005**, *240*, 96–100.
[5] Feynman, R. P.; Hibbs, A. R. *Quantum Mechanics and Path Integrals*; McGraw-Hill: New York, 1965; Chapt. 10, Sect. 3, pg. 281.
[6] Nicholson, D.; Parsonage, N. G. *Computer Simulation and the Statistical Mechanics of Adsorption*; Academic Press: London, 1982; Chapt. 3, Sect. 4, pg. 97.
[7] Belof, J. L.; Space, B. Massively Parallel Monte Carlo (MPMC). Available on GitHub, `https://github.com/mpmccode/mpmc`.
[8] Applequist, J.; Carl, J. R.; Fung, K.-K. *J. Am. Chem. Soc.* **1972**, *94*, 2952–2960.
[9] Thole, B. *Chem. Phys.* **1981**, *59*, 341 – 350.
[10] Bode, K. A.; Applequist, J. *J. Phys. Chem.* **1996**, *100*, 17820–17824.
[11] Dinh, T.-L.; Huber, G. A. *J Math. Modell. Algorithms* **2005**, *4*, 111–128.
[12] Belof, J. L. Theory and simulation of metal–organic materials and biomolecules. Ph.D. thesis, University of South Florida, 2009.
[13] Belof, J. L.; Stern, A. C.; Eddaoudi, M.; Space, B. *J. Am. Chem. Soc.* **2007**, *129*, 15202–15210, PMID: 17999501.
[14] Forrest, K. A.; Pham, T.; McLaughlin, K.; Belof, J. L.; Stern, A. C.; Zaworotko, M. J.; Space, B. *J. Phys. Chem. C* **2012**, *116*, 15538–15549.
[15] Palmo, K.; Krimm, S. *Chem. Phys. Lett.* **2004**, *395*, 133–137.
[16] Kirkpatrick, S.; C.D. Gelatt, J.; Vecchi, M. *Science* **1983**, *220*, 671–680.
[17] Yan, Y.; Lin, X.; Yang, S.; Blake, A.; Dailly, A.; Champness, N.; Hubberstey, P.; Schroder, M. *Chem. Commun.* **2009**, *1025*, 1025–1027.
[18] Rappé, A. K.; Casewit, C. J.; Colwell, K. S.; Goddard, W. A.; Skiff, W. M. *J. Am. Chem. Soc.* **1992**, *114*, 10024–10035.
[19] van Duijnen, P. T.; Swart, M. *J. Phys. Chem. A* **1998**, *102*, 2399–2407.
[20] Buch, V. *J. Chem. Phys.* **1994**, *100*, 7610–7629.
[21] Belof, J. L.; Stern, A. C.; Space, B. *J. Chem. Theory Comput.* **2008**, *4*, 1332–1337.
[22] Yan, Y.; Telepeni, I.; Yang, S.; Lin, X.; Kockelmann, W.; Dailly, A.; Blake, A.; Lewis, W.; Walker, G.; Allan, D.; Barnett, S.; Champness, N.; Schroder, M. *J. Am. Chem. Soc.* **2010**, *132*, 4092–4094.